Cumhuriyet Sci. J., 46(2) (2025) 274-285
DOI: https://doi.org/10.17776/csj.1599148

Cumhuriyet Science Journal

| csj.cumhuriyet.edu.tr | Founded: 2002 ISSN: 2587-2680 e-ISSN: 2587-246X Publisher: Sivas Cumhuriyet University

Investigation of a Stable Interaction of Levothyroxine with AFP through Molecular Modelling

Emel Akbaba[1,a], Deniz Karataş[2,b,*], Ataman Gönel[3,c], Ezgi Soylu[2,d], Beste Kiraz[2,e], Yusur Almahdi[2,f]

[1]*Department of Medical Biology, Faculty of Medicine, Kırıkkale University, Kırıkkale, 71450, Türkiye*

[2]*Department of Bioengineering, Faculty of Engineering and Natural Sciences, Manisa Celal Bayar University, Manisa, 45140, Türkiye*

[3]*Department of Biochemistry, Faculty of Medicine, Sanko University, Gaziantep, 27580, Türkiye*

**Corresponding author*

Research Article

History
Received: 12/12/2024
Accepted: 19/05/2025

ABSTRACT

Thyroid dysfunctions are common all over the world, and accordingly, the use of thyroid drugs has increased. Incorrect measurement of tumor markers may lead to missed cases of cancer. We hypothesized that the interaction between tumor markers and thyroid medications could lead to decreasing measurement of tumor markers in serum. The most used cancer markers are CA19-9, CA125, CEA, PSA, and AFP molecules. In this study, the molecular interactions of these markers with the thyroid medications of levothyroxine, methimazole, and propylthiouracil were investigated via molecular docking and dynamics simulations. In the molecular docking studies, levothyroxine was shown to interact with AFP, CEA, and CA15-3 in low concentrations. As a result of the MD simulations, the AFP/LEVO model exhibited the highest level of interaction. For instance, while the RMSD values of AFP/Levothyroxine complex were consistently around 0.7, and for the others they were observed above 1. This tight binding was reflected in interaction energies, with the total interaction in the AFP/Levothyroxine model computed as -192.04 kJ/mol. In contrast, for CA15-3/Levothyroxine and CEA/Levothyroxine complexes, these values were calculated as -135.26 and -88.56 kJ/mol, respectively. The SASA analysis also suggested the superiority of AFP/Levothyroxine complex due to ligand masking and a decrease in standard deviation, as the SASA mean difference area was found to be -0.46. This unique and only study elucidates the interactions between drugs used in thyroid cancer and biomarkers at the atomistic level. This clarity suggests a potential to mitigate misunderstandings that may arise in clinical and experimental studies.

Keywords: Levothyroxine, AFP, CEA, CA 15-3, Molecular modelling.

[a] *eakbaba@kku.edu.tr* *https://orcid.org/0000-0003-4915-5153*
[b] *deniz.karatas@cbu.edu.tr* *https://orcid.org/0000-0002-8176-4883*
[c] *catamangonel@gmail.com* *https://orcid.org/0000-0001-7200-1537*
[d] *211208006@ogr.cbu.edu.tr* *https://orcid.org/0000-0003-1322-580X*
[e] *160323017@ogr.cbu.edu.tr* *https://orcid.org/0009-0003-0125-8791*
[f] *221290005@ogr.cbu.edu.tr* *https://orcid.org/0009-0003-9569-3777*

Introduction

Thyroid function abnormalities are commonly encountered in general practice. Hypothyroidism and hyperthyroidism commonly arise from pathological processes within the thyroid gland. The diagnosis of thyroid dysfunction is predominantly based on biochemical confirmation [1]. Thyroid disfunction occurs much more often in females than males, with close to a million people being treated for hypothyroidism [2]. In iodine-replete populations, thyroid dysfunction is most commonly due to thyroid autoimmunity. The established treatment of hypothyroidism is carried out with levothyroxine [3]. Hyperthyroidism, on the other hand, is an excessive concentration of thyroid hormones in tissues causing a characteristic clinical state [4]. Hyperthyroidism caused by overproduction of thyroid hormones are commonly treated with antithyroid medications, methimazole and propylthiouracil [5].

Alteration of glycosylation, which occurs early in cancer, results in the production of tumor-associated glycans or glycoproteins. These molecules are subsequently secreted or membrane-shed into the blood stream and thus serve as tumor-associated markers. These glycosylation markers, applicable for detection and monitoring of cancer, include CA 19-9, CA 125, CEA, PSA, and AFP. Because of their specific affinity to distinct sugar moieties, lectins are useful for developing assays to detect these tumors associated with glycans and glycoproteins in clinical samples. As such, various enzyme-linked lectin assays have been developed for diagnosis, monitoring and prognosis [6].

Carbohydrate antigen 19-9 (CA 19-9) is a cell surface glycoprotein complex, most commonly associated with pancreatic ductal adenocarcinoma. Structurally, it is a tetrasaccharide carbohydrate with a transmembrane protein skeleton and extensively glycosylated extracellular oligosaccharide chains. CA 19-9 is also used as a biomarker for gastrointestinal (such as colorectal and oesophageal cancers), urological, gynecological, pulmonary, and thyroid cancers [7]. CEA and CA 15-3 are generally associated with breast cancer [8]. Furthermore, CA 125 has been a valuable indicator for evaluating the efficacy of treatment and prognosis in ovarian cancer [9]. Alpha-fetoprotein (AFP) is considered as a diagnostic and prognostic cancer marker for

hepatocellular carcinoma which is one of the most common malignant tumors in the World [10]. Prostate specific antigen (PSA) is generally known as prostate cancer antigen [11]. Therefore, the specificity of cancer antigens is variable.

Molecular docking is a method which analyses the conformation and orientation of molecules (ligands) into a macromolecular target (receptor). Molecular docking is extensively used to hypothesize interaction modes and better characterize the ligand-receptor interactions [12]. Indeed, molecular docking is among one of the most popular and successful structure-based *in silico* methods, which help predict the interactions occurring between molecules and biological targets. Based on the protein structures, many possible poses of ligand are generated. Therefore, the first step is predicting the molecular orientation of a ligand within a receptor, and then estimating their complementarity through the use of a scoring function [13]. This molecule/protein complex must form a stable complex [14]. The binding free energy directly mirrors the ability of the ligand to interact with the protein, and is, therefore, regarded as the key quantity in studies of molecular recognition and association phenomena. The lowest the binding energy, the highest the binding affinity is [15]. The important energetic factors for protein–ligand binding, such as hydrogen bonds, and hydrophobic effects are also used to predict binding affinity [16]. Molecular dynamics (MD) simulations, on the other hand, predict how every atom in a protein or other molecular system will move over time, based on a general model of the physics governing interatomic interactions. These simulations can capture a wide variety of important biomolecular processes, including conformational change, ligand binding, and protein folding, revealing the positions of all the atoms at femtosecond temporal resolution [17]. In this study, MD simulations were performed to evaluate the stability of ligand/receptor complexes. Recently, the molecular interactions between propylthiouracil and thyroid peroxidase, a key enzyme in thyroid hormone synthesis has investigated with MD and docking. The aim is to elucidate the binding mechanism of propylthiouracil as an inhibitor of thyroid peroxidase at the atomic level. The study clarifies the key interactions, like hydrogen bonds, and hydrophobic interactions, that contribute to propylthiouracil's inhibitory activity [18]. In another recent study utilizes an integrated computational approach to explore the molecular mechanisms by which perfluorooctane sulfonic acid induces thyroid toxicity. Molecular docking and molecular dynamics simulations revealed the potential binding interactions between perfluorooctane sulfonic acid and key thyroid-related proteins, such as thyroid peroxidase and thyroid hormone receptors [19]. Another paper used molecular dynamics simulations to investigate the molecular mechanisms behind the resistance to resmetirom, a selective thyroid hormone receptor beta agonist, in certain contexts. The simulations identified key amino acid residues and interactions that are crucial for resmetirom binding and how these are affected in resistant variants [20]. Another paper suggested that two common anti-thyroid drugs, methimazole and propylthiouracil, inhibited the enzymatic activity of thyroid peroxidase in the results which obtained through computational study [21]. One another theoretical and experimental study showed the interaction between levothyroxine, and bovine serum albumin [22]. *In silico* studies on biomarkers and thyroid cancer have also become popular in recent years. One comparative modelling study investigated the role of Iron-Sulfur Cluster Assembly 1 (ISCA1) across various cancer types, with a specific focus on its correlation with ferroptosis-related genes and its potential as a biomarker in thyroid carcinoma. [23]. Another study investigated a multi-omics network approach to identify systems biomarkers for papillary thyroid cancer prognosis and treatment. [24]. Another study employed gene-expression profile analysis to identify potential biomarkers for thyroid carcinoma. [25]. In the meantime, another study combined network pharmacology and molecular docking to investigate the mechanisms by which polybrominated diphenyl ethers to induce thyroid dysfunction. [26]. Another study performed a comprehensive, large-scale transcriptomic analysis of RNAs in thyroid cancer to identify pathological biomarkers related to the tumor immune microenvironment and to explore potential target therapies [27]. Although there is a body of research on the interactions between thyroid cancer therapeutics and diverse protein targets, theoretical studies pertaining to the interaction of these drugs with glycosylation markers are notably absent from the current literature. Therefore, in this study, our hypothesis was as follows: The medications used for thyroid disorders may interact with tumor markers, preventing their detection in blood tests. Given the widespread use of thyroid medications in the population, the suppression of tumor markers could adversely affect cancer diagnosis or follow-up treatments. The interactions of thyroid drugs with tumor markers may alter the serum levels of tumor antigens, which may cause a possible case of cancer to be missed as a result. Therefore, we investigated the interactions between certain thyroid medications and the tumor markers through the use of molecular docking, and dynamics simulations.

Materials and Methods

Protein Preparation

The molecular structures of tumor markers were imported from PDB (Protein Data Bank). The chosen tumor markers are AFP (PDB id: 3MRK), CA125 (PDB id: 1IVZ), CEA (PDB id: 5DZL), PSA (PDB id: 1GVZ), and CA15-3 (PDB id: 6BSC). Only CA19-9 was imported from PubChem (PubChem CID: 643993). All macromolecules were exhibited in alpha helixial and beta sheet structures, except CA19-9 which is the only non-protein cancer marker studied in this research. CA19-9 is a carbohydrate antigen; therefore, it is displayed in sticks with the colors specific to atom type (Figure 1).

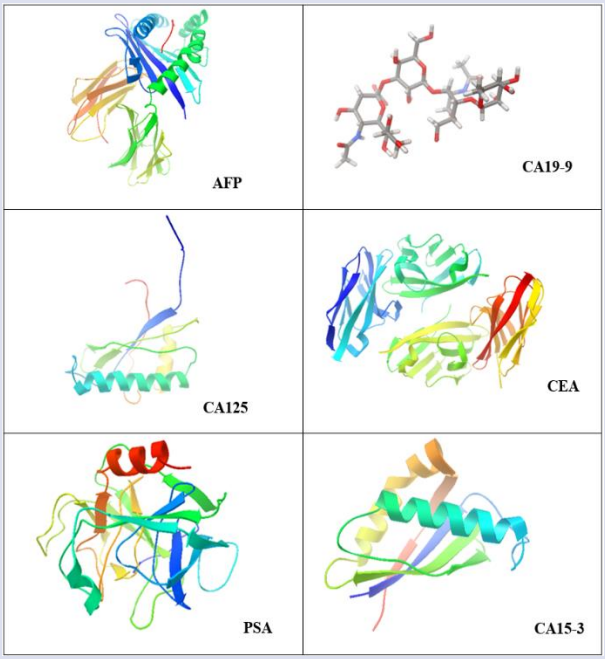

Figure 1. The structures of tumor markers are shown in rainbow form except CA19-9 of which is displayed in balls and sticks. Grey, red, white, and blue colors for CA19-9 represent carbon (C), oxygen (O), hydrogen (H) and nitrogen (N), respectively.

Before starting docking, water molecules and other irrelevant ligands were removed. Then marker molecules were prepared as a PDBQT file format using AUTODOCK TOOLS [28]. The missing residuals were checked and repaired. Hydrogen atoms were added to the dangling bonds. In the following step, Kollman charges were assigned and added to the marker molecules.

Ligand Preparation

The molecular structures of all drugs were imported from the PubChem databank, saved in .sdf format. The file in SDF format was converted to PDBQT format using the OpenBabelGUI (ObGUI) program [29]. The structures of the ligands (drugs) are shown in the Figure 2.

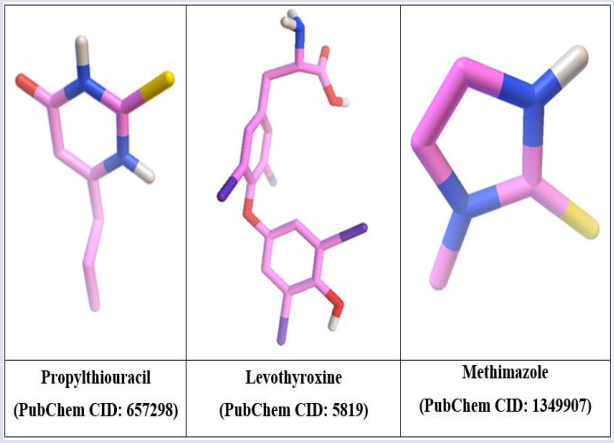

Figure 2. The structures of drugs are shown in ball-stick model. White, red, pink, purple, blue, and yellow colors represent hydrogen (H), oxygen (O), carbon (C), iodine (I), nitrogen (N), and sulfur (S), respectively.

Launching Autogrid

The number of grid box points and xyz coordinates adjusted that completely cover the macromolecule structure entered from the grid box section. The grid parameter file (GPF) was saved with the entered values. All GPF parameters were illustrated in Table 1. These parameters are the default values generated by the AutoDock Tools software subsequent to the definition of the grid box. Before selecting, GPF file to run autogrid, autogrid4.exe program was launched. As GPF file was selected from working directory, at the same time a grid log file (GLG) with the same name was automatically generated. After the running finished all parameters, such as atom types, grid box details, dielectric constants, and lowest pairwise-atomic interaction energies.

Table 1. GPF parameters for ligand/marker models.

DRUG	MARKER	# of Grid Points (xyz)	Spacing	xyz Grid Center Coordinates(Å)
Propylthiouracil	AFP	126 126 126	0.55	7.391 x -0.582 x 9.49
	CA 19-9	50 50 50	0.375	-1.154 x 5.576 x -2.915
	CA 125	126 126 126	0.55	-1.929 x 11.891 x -4.083
	CEA	126 126 126	0.575	11.566 x -10.159 x 1.684
	PSA	126 126 126	0.5	11.3 x 23.915 x 24.743
	CA 15-3	100 100 100	0.375	-19.265 x 11.673 x 4.338
Levothyroxine	AFP	126 126 126	0.55	7.391 x -0.582 x 9.49
	CA 19-9	50 50 50	0.375	-1.154 x 5.576 x -2.915
	CA 125	126 126 126	0.55	-1.929 x 11.891 x -4.083
	CEA	126 126 126	0.575	11.566 x -10.159 x 1.684
	PSA	126 126 126	0.5	11.3 x 23.915 x 24.743
	CA 15-3	110 110 110	0.5	-19.265 x 11.673 x 4.338
Methimazole	AFP	126 126 126	0.55	7.391 x -0.582 x 9.49
	CA 19-9	50 50 50	0.375	-1.154 x 5.576 x -2.915
	CA 125	126 126 126	0.55	-1.929 x 11.891 x -4.083
	CEA	126 126 126	0.575	11.566 x -10.159 x 1.684
	PSA	126 126 126	0.5	11.3 x 23.915 x 24.743
	CA 15-3	100 100 100	0.375	-19.265 x 11.673 x 4.338

All the values of grid points, spacing, and grid center coordinates of propylthiouracil and methimazole are identical as shown in Table 1. However, values of grid center points and spacing of CA15-3/levothyroxine complex are different from that of CA15-3/propylthiouracil and CA15-3/levothyroxine complexes. The reason for this exceptional situation is molecular size and structurally complexity of Levothyroxine.

Molecular Docking

Apolar hydrogens cannot be read in XRD. To get exact results with XRD, nonpolar hydrogens were neglected. OpenBabel GUI (ObGUI) was used to calculate the minimum (most stable) charges. The codes of the drugs were inserted into the input format section of the ObGUI. The file type was selected as SDF. The output file was then saved as ".pdbqt" format in the relevant drug folder. Then the AutoDock program was started. Before submitting docking, macromolecule was selected to set receptor molecules as rigid body. Genetic algorithm (GA) was selected as search parameters. The number of runs and population size were selected as 100, and 300, respectively. Furthermore, the number of evals was chosen as long level. Hybrid Lamarckian and GA parameters were assigned, and the input file was saved as docking parameter file (DPF) (Table 2). Finally, DPF was selected to launch docking [30].

Table 2. DPF parameters for ligand/marker models.

Program	Autodock4.exe
Search Parameters	Lamarckian Genetic Algorithm
# of Run	100
# of Generations	27000
Maximum # of Energy Evaluations (Long level)	25000000
Population Size	300

For the analysis of the results, the run number where the lowest binding energy occurs should be entered in the conformations section and visualized. In the result pop out, all RMSD results were exhibited in detail.
The free binding energy (BE) calculation was carried out as follows.

Estimated Free Energy of Binding = (1) + (2) + (3) - (4)
(1): Final Intermolecular Energy = [vdW + Hbond + desolvation Energy] + Electrostatic Energy; (2): Final Total Internal Energy; (3): Torsional Free Energy; (4): Represents Unbound System's Energy = [(2) Final Total Internal Energy].

Molecular Dynamics (MD)

The ligand/receptor complexes with the highest binding affinities were further evaluated via MD simulations which were conducted using the GROMACS program to elucidate the interaction regions and energies in aqueous environments with full atomic mobilities as compared to molecular docking. Prior to initiating MD simulations, all atoms in the model were assigned using the CHARMM36 force field recommended for protein-ligand complexes. The TIP3P water model was selected for the solvent environment. Subsequently, a simulation box in the form of a dodecahedron was constructed, considering the protein structure, after merging the ligand molecule prepared on the swissParam website with the protein. Ion addition was performed to neutralize the ligand/protein simulation boxes containing water, followed by sufficient minimization using the steepest descent algorithm in 3D periodicity to reduce over-accessed energy on atoms and prepare the supercell for simulation. Next, equilibration was carried out in NVT and NPT ensembles for each of the three boxes, with 100 picoseconds (ps) each, followed by independent 50-nanosecond (ns) simulations. Moreover, temperature and pressure were maintained constant during the simulation via a modified Berendsen thermostat and the Parrinello-Rahman barostat. A temperature of 300 K and a pressure of 1 bar were applied. Short-range van der Waals forces were truncated at a cutoff distance of 1.2 nm, and long-range electrostatic forces were computed employing the Particle Mesh Ewald summation [23, 31]. To analyze molecular interactions and sizes between protein and ligand, RMSD, RMSF, radius of gyration, SASA, RDF, and interaction energy analyses were successively performed. In all relevant analyses, the entire ligand molecule was selected in contrast to the protein backbone for thorough examination.

Results and Discussion

In silico studies revealed new insights about the possible binding mode of different compounds with receptors [32]. This research aimed to study possible interactions of the selected drugs used in hyperthyroidism or hypothyroidism with the serum tumor markers via molecular docking analysis. Propylthiouracil (PRO) and methimazole (MET), the drugs used in hyperthyroidism, and levothyroxine (LEVO) which is used in hypothyroidism were chosen as the ligand molecules. On the other hand, AFP, CA19-9, CA125, CA15-3, CEA, and PSA were selected as the receptors which are commonly known as tumor antigens routinely used to predict various cancers. The elevated levels of tumor markers could be a sign of cancer, therefore, should not be underestimated. Tumor markers can be evaluated by a blood test which is an easy and inexpensive method. This study aims to question the reliability of tumor marker measurement tests in people using the selected thyroid medications. The possible interactions of tumor markers and thyroid drugs are possibly change the serum levels of the antigens. One of the possible outcomes of the tumor marker with drug interaction is a decrease in serum tumor marker levels, which may be interpreted as ignoring the cancer, which may have devastating outcomes. Thyroid disease is common in older adults. Up to 5%, and 2.3% of older people are diagnosed with hypothyroidism and hyperthyroidism, respectively [33]. It is obvious that

cancer cases also increase with age. The interactions of thyroid medications with cancer markers could result in the elimination or delay of cancer diagnosis in the case of an elderly using thyroid drugs with no symptoms of cancer, who only has cancer marker bioassays. Therefore, it is essential to make certain that the medications used to treat thyroid diseases do not have any kind of interaction with the cancer markers.

In all the selected tumor markers, the simplest and smallest marker is CA19-9 whereas AFP, CEA and PSA are more complex and bulkier than others (Figure 1). All examined ligand molecules with the polar hydrogens were depicted in Figure 2. Four iodine atoms just exist covalently in LEVO, the biggest, bulkiest, and longest ligand whereas sulfur belongs to the other drugs, relatively smaller and simpler structures (Figure 2).

Molecular Interactions of Markers and PRO

The molecular interactions of marker and PRO from the total 100 runs are shown in Table 3.

Table 3. Molecular interactions of markers and PRO.

MODEL	BE from Lowest to Highest (kcal/mol)	IC From Lowest to Highest (mM)	Number of Clustering	Lowest Binding Run	Detected H-bonds (Å)
AFP/PRO	(-5.51)	(0.09)	8	72	No H-Bond formed
	(-4.79)	(0.31)			
CA19-9/PRO	(-3.88)	(1.44)	2	11	(1.971)
	(-3.70)	(1.95)			(2.131)
CA125/PRO	(-3.95)	(1.28)	15	15	No H-Bond formed
	(-3.57)	(2.42)			
CEA/PRO	(-4.40)	(0.59)	19	18	ASP82:A(2.133)
	(-3.80)	(1.65)			
PSA/PRO	(-5.39)	(0.11)	10	16	LYS95F:A(1.965)
	(-4.00)	(1.16)			
CA15-3/PRO	(-4.67)	(0.37)	9	3	PHE1094:A (2.234)
	(-3.78)	(1.70)			

The amino acids contributing to the H-bonds which are listed in Table 3 are also shown in Figure 3. The lowest and highest binding energies of AFP/PRO model were determined to be -5.51 and -4.79 kcal/mol, respectively. Clearly, less than 1 kcal/mol difference was obtained between the lowest and highest binding energies of AFP/PRO model. Furthermore, AFP/PRO complex was found to be clustered in 8 sites out of 100 conformations. No hydrogen (H) bond was observed in this model, however, hydrophobic interactions with PHE22 and PRO20 which exist on A chain of AFP with PRO were determined. Also, other intermolecular interactions were observed in PRO with the residues SER11A, GLU19A, SER38A, SER71A, GLN72A, and ARG75A of AFP. Furthermore, a low inhibition constant (IC) value (0.09 mM) was found in AFP/PRO complex. Therefore, all these factors contributed to the low binding energy, suggesting AFP as the most favorable tumor marker with the interaction of PRO. A recently published study reported docking scores for Propylthiouracil spanning from -4.485 to -5.144 kcal/mol across ten distinct models, which closely align with the results obtained in our current research [18]. The aforementioned study highlighted the substantial interaction exhibited by the Propylthiouracil molecule with the thyroid hormone receptor. Another study, employing not only docking but also MD simulations, demonstrated a considerably strong interaction between the same drug and the same receptor [21].

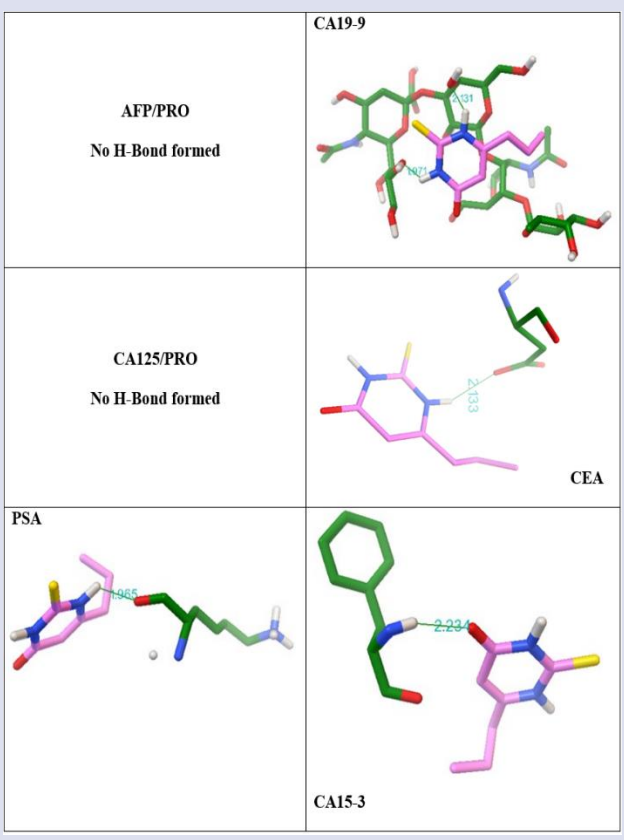

Figure 3. The marker/PRO interaction poses. The amino acids contributing to H-bonds are shown in green. Propylthiouracil (PRO) is shown in pink.

PSA/PRO model was also found to have low binding free energy (-5.39 kcal/mol) with one H-bond interaction. The IC value of this model was shown to be 0.11 mM. Furthermore, CA15-3/PRO model which has a binding energy of -4.67 kcal/mol displayed one H-bond as well as low IC value (0.37 mM). π-cation interactions were also observed in PRO with LYS1093A, in addition to hydrophobic interactions with PHE1054A, PRO1061A, and PRO1096A of CA 15-3. Furthermore, other intermolecular interactions were predicted between PRO and CA 15-3 with GLU1059A, TYR1066A, and ARG1095A residues. The marker/PRO poses displaying the lowest binding energies are shown in Figure 3. H-bonds were determined in all models except AFP/PRO and CA125/PRO. The effective driving forces in AFP/PRO and CA125/PRO models were determined as van der Waals interactions (-5.92 and -4.41 kcal/mol, respectively), while electrostatic interactions remained at minimum levels (-0.19 and -0.05 kcal/mol, respectively). However, in the other marker/PRO models, the effective driving forces were determined to be H-bonds and van der Waals interactions, with the minimum electrostatic contribution. Such hydrogen bonding and hydrophobic interactions have also been identified by using molecular docking and dynamics investigations involving PRO, which have further elucidated their function in regulating the interactions with the receptor [18, 21].

Molecular Interactions of Markers and LEVO

Molecular interactions of markers and LEVO are shown in Table 4.

Table 4. Molecular interactions of markers and LEVO.

MODEL	Binding Energy (kcal/mol)	Inhibition Constant (mM)	Number of Clustering	Lowest Binding Run	Number of Detected H-bonds (Å)
AFP/LEVO	(-8.10) (-4.54)	(0.001) (0.4)	60	83	ASP30:A(2.084) GLY237:A(1.968) ARG12:B(1.992)
CA19-9/LEVO	(-4.53) (-3.01)	(0.478) (6.21)	22	36	2.239
CA125/LEVO	(-5.30) (-3.16)	(0.063) (4.86)	67	73	ASP95:A(2.129) ARG120:A(2.168) ARG96:A(2.152)
CEA/LEVO	(-8.60) (-4.51)	(0.0004) (0.494)	51	78	THR4:B(2.131) THR101:B(1.813) SER6:C(2.103)
PSA/LEVO	(-7.16) (-4.48)	(0.005) (0.5)	57	48	LYS95F:A(1.722) ARG150:A(2.068)
CA15-3/LEVO	(-8.35) (-5.73)	(0.0008) (0.06)	37	8	No H-Bond formed

Clearly seen from Table 4 that low binding energies were determined in all models of LEVO/marker. Figure 4 shows the best conformations of LEVO with the markers. A combined experimental and computational study into the molecular interplay between levothyroxine and thyroid hormones revealed a considerably high degree of interaction. Moreover, the binding affinity of the lowest energy conformer was determined to be -6.4 kcal/mol through docking simulations. The underlying interactions responsible for this affinity were illustrated as predominantly involving hydrogen bonds and hydrophobic forces [22].

The highest affinity between LEVO and tumor markers was determined to be in LEVO/CEA model which displayed an incredibly low binding free energy as -8.60 kcal/mol. H-bond interactions were predicted in LEVO with the residues THR4B, THR 101B, and SER6C of CEA. Furthermore, hydrophobic interactions with LEU2B, PHE9C, and ALA100B residues as well as other intermolecular interactions with ASN42A, GLN1B, GLU99B, THR3C, THR4C, GLN103C of CEA also contributed to the low binding energy. IC value of LEVO/CEA complex was found to be 0.0004 mM which is the lowest in all LEVO/marker models.

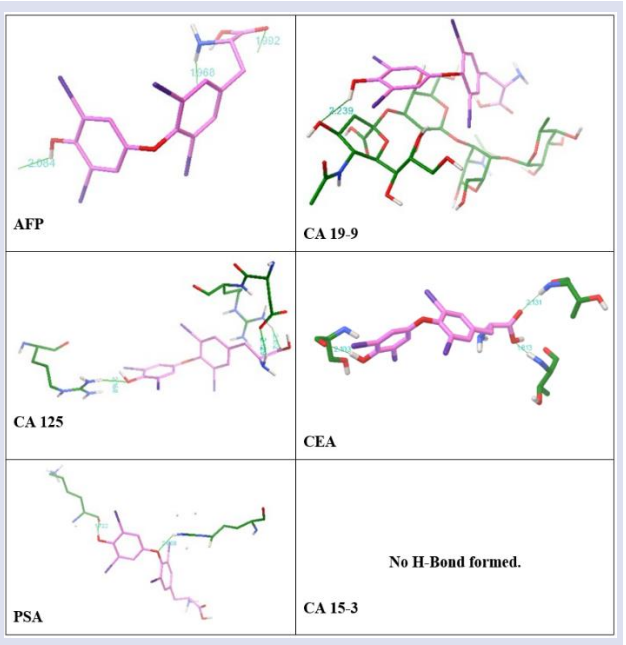

Figure 4. The LEVO/marker interaction poses. The amino acids are shown in green. Levothyroxine (LEVO) is shown in pink.

On the other hand, LEVO/CA 15-3 model was shown to display the second lowest binding energy (-8.35 kcal/mol). Although no H-bonds were predicted in LEVO with CA 15-3, hydrophobic interactions were observed with PHE1042A, LEU1078A, GLY1088A, LEU1089A, ALA1106B and ALA1106B, in addition to other intermolecular interactions with GLN1070A, SER1074A, SER1090A, ASN1091A, THR1104B amino acids of CEA. The low IC value of LEVO/CEA complex was noticed as 0.0008 mM. Therefore, CEA and CA 15-3 were suggested as the most favorable tumor markers in the interactions with LEVO. Furthermore, LEVO displayed low binding free energies of -8.10 kcal/mol and -7.16 kcal/mol with AFP and PSA, respectively. ASP30A, GLY237A, and ARG12B residues of AFP constituted H-bond interactions. Also, hydrophobic interactions in LEVO with TRY27A, LEU65B, and TYR67B were determined, in addition to other intermolecular interactions with THR31A, GLN32A, ARG48A, and SER52B residues of AFP. On the other hand, H-bond interactions in LEVO with LYS 95FA and ARG 150 A of PSA were observed. MET60, and LEU95I residues of PSA were observed to form hydrophobic interactions with LEVO. Also, other intermolecular interactions were observed between LEVO and PSA with HIS35, HIS39, GLN41, HIS57, and LYS95G residues. Therefore, the above-mentioned interactions of LEVO with AFP and PSA contributed to the low binding energies.

Among all LEVO/marker models, a relatively low binding affinity between LEVO and CA125 was observed as -5.30 kcal/mol binding energy. However, many bonding interactions were predicted in this complex such as H-bond interactions with residues ASP95A, ARG120A and ARG96A at high distances. On the other hand, hydrophobic interactions in LEVO were observed with VAL97, TYR100, PHE124, and VAL125, in addition to intermolecular interactions with ASP95, TYR100, and ARG120 residues of CA125. Therefore, although binding score of LEVO/CA125 complex was shown to be relatively low, many bonding interactions in this complex suggest good binding affinity.

As it can be seen from Table 4, high number of clustering in all LEVO/marker models were obtained. For example, in LEVO/CEA model, number of clustering was determined to be 51 in 100 conformations, suggesting many binding sites of the markers. Although LEVO is the bulkiest ligand in this study, substantially low binding energies with the markers were shown. LEVO is the only ligand in this study, possessing iodine residue and many polar hydrogens. Probably, these factors increased the affinity of LEVO to tumor markers, especially CA15-3, CEA, AFP, and PSA.

H-bonds and van der Waals interactions were found to be the effective driving forces in the interactions of LEVO with tumor markers. However, electrostatic interactions remained at minimum levels in all LEVO/marker complexes.

Molecular Interactions of Markers and MET

Molecular interactions of markers and MET are given in Table 5. The binding energy of MET with PSA was observed to be -3.70 kcal/mol which is the lowest value within all MET/marker complexes. No H-bond interactions of MET with PSA were predicted. Furthermore, MET was found to represent a binding energy of -3.22 kcal/mol with CA125 which is also considered as low binding affinity. A H-bond interaction of MET was observed with VAL 125A of CA 125. Also, the IC value (4.39 mM) was determined to be moderately higher than PSA/MET model (1.94 mM). Figure 5 illustrates the best conformations of MET with the tumor markers. Clearly, MET did not reveal good binding affinities with any of the tumor markers in 100 conformations. Therefore, MET is not considered to be a favorable ligand for the studied tumor markers. With only one polar hydrogen, MET is the smallest ligand in this study. Possibly, the interactions of MET with the chosen markers are constrained by the presence of a single polar hydrogen. *In silico* study involving methimazole have demonstrated its interaction with thyroid peroxidase enzymes, mediated by hydrogen bonds and hydrophobic forces [21].

Table 5. Molecular interactions of markers and MET.

MODEL	Binding Energy (kcal/mol)	Inhibition Constant (mM)	Number of Clustering	Lowest Binding Run	Number of Detected H-bonds (Å)
AFP/MET	(-3.10) (-2.87)	-5.37 -7.88	4	39	HIS70:A (1.521)
CA19-9/MET	(-2.58)	12.85	1	65	-2.134
CA125/MET	(-3.22) (-2.84)	-4.39 -8.27	3	83	VAL125:A (1.825)
CEA/MET	(-3.06) (-2.74)	-5.73 -9.76	12	97	No H bond
PSA/MET	(-3.7) (-3.32)	-1.94 -3.67	7	95	No H Bond
CA15-3/MET	(-3.09) (-2.93)	-5.46 -7.11	2	84	ASN1091:A (2.021)

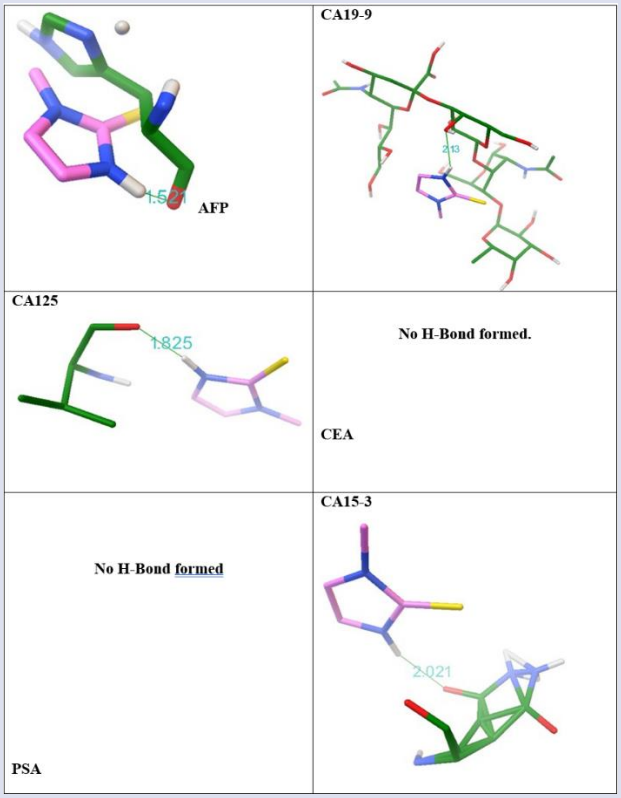

Figure 5. The marker/MET conformations with the lowest binding energies. The amino acids are shown in green. Methimazole (MET) is shown in pink.

Other forces affecting the molecular interactions between the tumor markers and the drugs, apart from the H-bond interactions, are given in Figure 6. The van der Waals spheres forming the molecular surface and close contacts of the left images are removed in the right images so that the π-cation yellow light beam can be seen. Two π-cation interactions occurred in the CA15-3/PRO model, while one was formed in CA15-3/LEVO. As a result of the docking, it was observed that the other parameters affecting the molecular interactions apart from the H-bond were π-cation and van der Waals interactions.

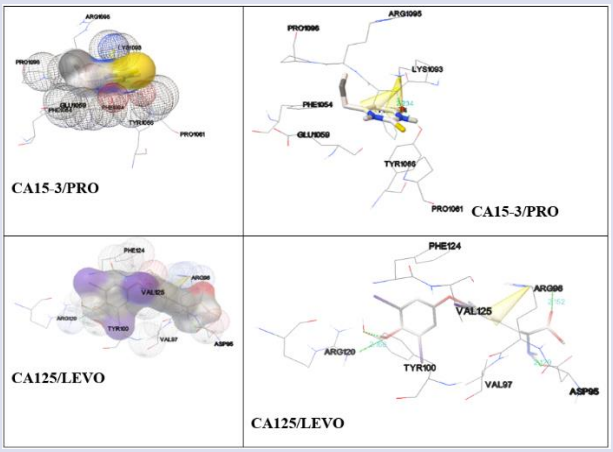

Figure 6. The molecular shape of CA15-3/PRO model shows amino acids causing hydrophobic interactions. The grey van der Waals spheres are carbonaceous region; red wireframe spheres are oxygen; the yellow region is sulfur, the purple spheres are iodine region, and the white spheres are hydrogenous region.

As a result, molecular docking analyzes revealed high binding affinities of LEVO to AFP, CA15-3, and CEA tumor marker proteins. Further, MD simulations were performed to support the stability of the aforementioned ligand/receptor interactions. ARG96 residue constituted π-cation interaction between LEVO and CA125, as well.

Structural and Dynamic Analyses

RMSD, RMSF and Rg graphs, which are indicators of structural changes and protein stability of LEVO, are given in Figure 7.

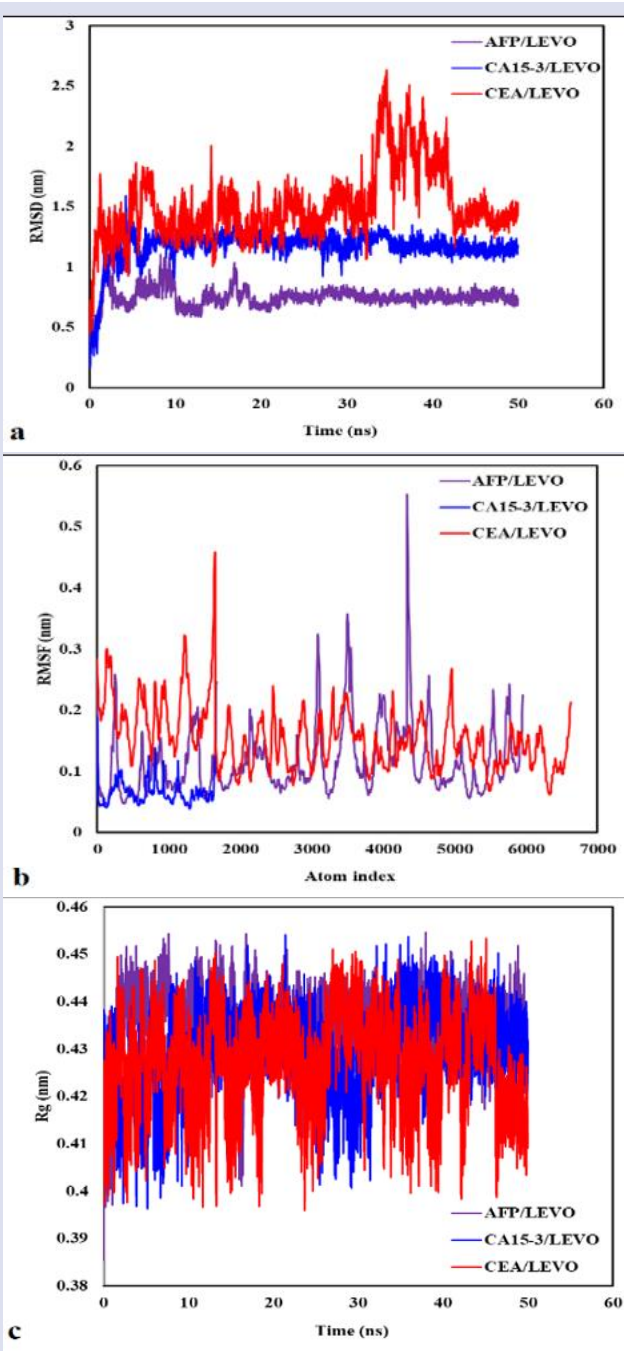

Figure 7. RMSD (a), RMSF (b), and Rg (c) graphs of AFP/LEVO, CA15-3/LEVO, and CEA/LEVO models.

RMSD (Root Mean Square Deviation) is the average measurement of atomic positions between two structures. In MD simulations, RMSD is employed to assess the similarity or dissimilarity between the generated protein and ligand complex and a reference

structure by comparing the variations in their positional alignment [34]. RMSD graphs facilitate the analysis of structural variations and stabilities in proteins and ligands. Additionally, they enable the interpretation of interactions between the ligand and protein throughout the simulation, as well as the observation and analysis of structural conformational changes during the binding of the ligand to the receptor [35].

It is a crucial type of graph for determining the equilibrium of the structure and dynamic stability. Figure 7a shows the RMSD graphs of AFP/LEVO, CA15-3/LEVO and CEA/LEVO complexes during a 50-nanosecond duration of MD simulation. The AFP/LEVO model exhibits a stable simulation, converging around 0.7 nm after the initial 10 ns and continuing steadily until completion. Similarly, the CA15-3/LEVO model stabilizes around 1.25 nm and continues consistently. In contrast, the CEA/LEVO model shows relatively larger fluctuations, reaching approximately 1.5 nm, with oscillations exceeding 2 nm observed between 35-45 ns of the simulation interval. This variation can be attributed to the presence of four chains in CEA, unlike the other models which have only one chain, and the stability of CEA appears to be influenced by the presence of the ligand. Indeed, in a study reporting the resolution as 3.4 Å in the X-Ray PDB validation report properties, it was observed that the resolution was notably lower, especially when compared to CA15-3 [36]. It is evident that the presence of the ligand affects the stability of the protein-ligand complex.

Root Mean Square Fluctuation (RMSF) denotes the calculation of atomic fluctuations in protein-ligand complexes generated during MD simulations over a specified time interval. The RMSF value allows for calculations regarding the extent to which the average positions of each structure deviate [34]. In MD simulations, the RMSF value provides information about the flexibility and conformational changes in specific regions of the protein, such as the binding site [37]. Figure 7b shows the RMSF graphs of AFP/LEVO, CA15-3/LEVO and CEA/LEVO complexes. Clearly, the CEA/LEVO model exhibits the highest fluctuations, attributed to the bulkier and more flexible nature of the CEA structure. The ordering of atom indices from large to small is a consequence of the CEA molecule having the longest total sequence length, followed by the sequence length of the single chain in AFP. The prominent peaks in AFP/LEVO correspond to atoms at indices 3088, 3503, and 4335. In CEA/LEVO, the most distinct peak is at index 1653, measuring 0.46 nm.

The gyration radius is utilized in MD simulations to discern the compactness of the protein-ligand complex, aiming to observe the shape and stability of the complex [38] [39]. This type of graph enables the assessment of the compactness of the protein-ligand complex. Gyration radius graphs corresponding to AFP/LEVO, CA15-3/LEVO and CEA/LEVO complexes are presented in Figure 7c. When examining the averages of the gyration radius (Rg) results, it is noted that their numerical average is approximately 0.43 nm for all models. However, as evident in Figure 7c, the CEA/LEVO complex exhibits a notably lower Rg value, especially in the last 4 ns of the simulation, compared to the others. This suggests that CEA is more flexible and disordered confirming the RMSD and RMSF results.

Solvent Accessible Surface Area (SASA)

SASA is the surface area accessible to the solvent molecules in a molecular system. SASA enables the measurement of the area accessible to the solvent in protein-ligand complexes. The determination of SASA is crucial for understanding protein folding and stability. Additionally, SASA reflects the hydrophobic compactness of protein structures [40].

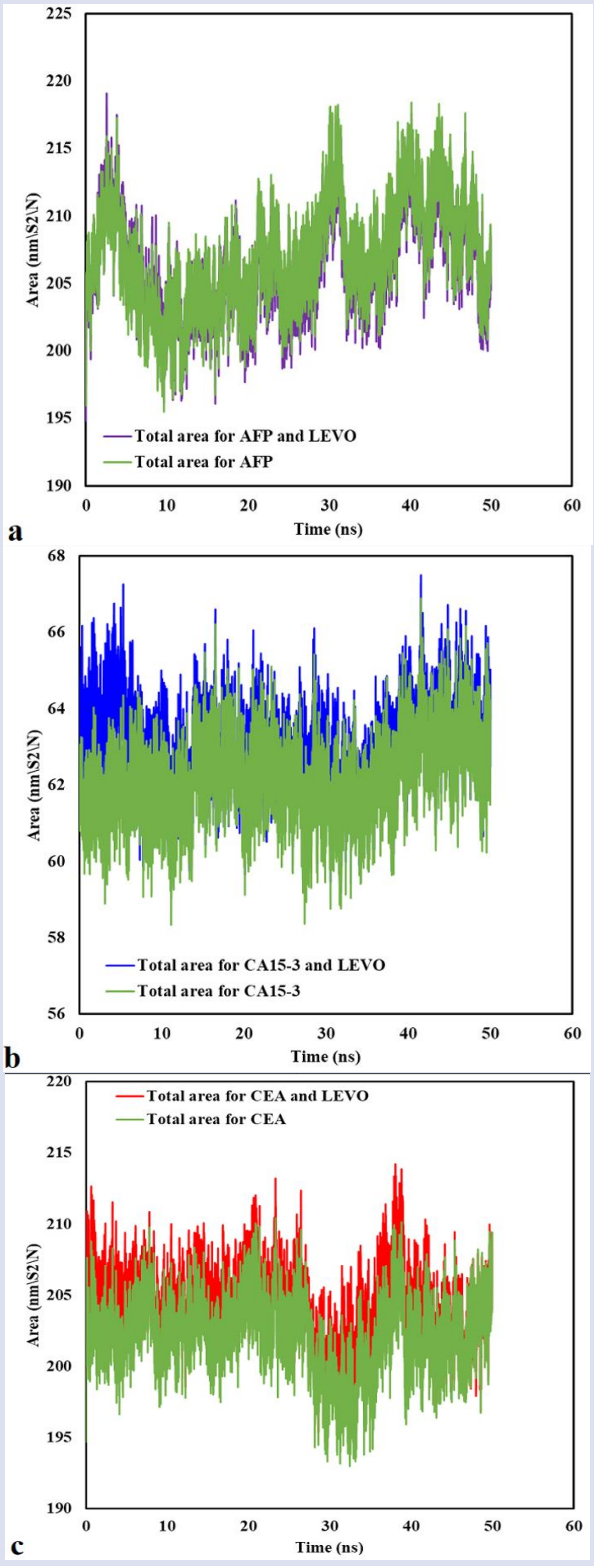

Figure 8. SASA curves for protein and protein/ligand models for the complexes of AFP/LEVO (a), CA15-3/LEVO (b), and CEA/LEVO (c).

In Figure 8, SASA graphs of protein-ligand complexes have been obtained to illustrate their behavior concerning solvent interactions. A slight decrease in SASA is observed in the presence of LEVO in the AFP/LEVO complex shown in Figure 8a. Indeed, the calculated difference in average areas is -0.46. Conversely, in the other two models, opposite results are obtained, with differences calculated as +0.80 and +2.13 for CA15-3/LEVO and CEA/LEVO complexes, respectively. According to these results, it can be inferred that the ligand masks the surface accessibility of the protein. On the other hand, the reason for the higher overall fluctuation areas in AFP is due to its having the shortest sequence length (57 amino acids) among the proteins. In the others, these fluctuation ranges are relatively less, especially in CA15-3. These minor fluctuations may suggest the formation of a stable complex between the ligand and the protein.

Radial Distribution Function (RDF) Analyses and Interaction Energies

The term RDF refers to measuring the distance distribution of a specific molecule with reference molecules. In MD simulations, the RDF graph enables the interpretation of protein-ligand interaction sites, interaction dynamics, binding regions, and stabilities [41]. In Figure 9, the RDF graph for LEVO with the receptors' backbone is provided.

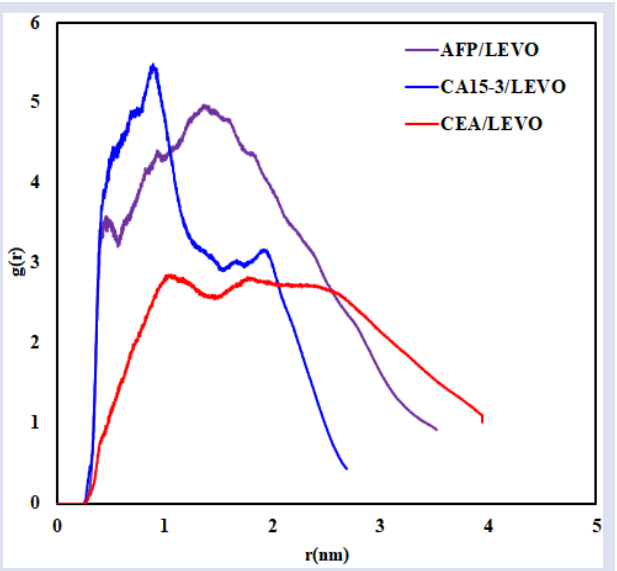

Figure 9. RDF graphs for AFP/LEVO, CA15-3/LEVO, and CEA/LEVO models.

The ligand exhibited its highest peak around 1 nm with the CA15-3 receptor, as indicated by the RDF results, highlighting this region as the most frequently occupied. In the AFP/LEVO model, the highest peak was observed around 1.6 nm, while in CEA/LEVO, a dominant and broad peak occurred in the range of 1-3 nm. These peaks and regions serve as clear evidence of the interaction between the ligand and the protein. To quantify these interactions, interaction energies between protein and ligand molecules were calculated, and the results are provided in Table 6.

Table 6. Total short range interaction energies and their contributions.

Energy, kJ/mol	AFP/LEVO	CA15-3/LEVO	CEA/LEVO
Coulombic	-78.13	-25.26	-23.17
Lenard-Jones	-113.91	-110	-65.39

Upon examining the results in Table 6, it can be asserted that the LJ parameter, and thus van der Waals interactions, are more effective. Regarding electrostatic interactions, the contribution is -78.13 kJ/mol in AFP/LEVO complex. In molecular docking results, however, CEA/LEVO exhibits the lowest total interaction energy. This observation may suggest that one of the influential parameters here is the hydrogen bonding.

Molecular docking and dynamics investigations were performed in this study, and the results showed that LEVO has a high affinity in low concentrations for binding to CEA, CA15-3, and AFP, which are all tumor markers. In particular, the MD results demonstrated that the LEVO/AFP complex exhibited a significant degree of stability while being simulated for fifty nanoseconds. As a result, we propose that the thyroid medicine LEVO interacts with AFP, which may result in a change in the amount of AFP that is present in the blood serum. The molecular structure of the protein will almost certainly undergo a change, whether it is in a single form or contained within a complex. That being the case, it is quite possible that the complex form of AFP is not detectable in blood serum. As a consequence of this, the amount of AFP that is present in the serum can appear to be quite low, which might lead to inaccurate findings.

Conclusion

In this study, molecular docking and dynamic studies have revealed the interactions of levothyroxine used in thyroid disfunction with tumor markers of CEA, CA 15-3, and AFP. Other than H-bond and van der Waals interactions, hydrophobic and π-cation interactions were also found to contribute this interaction. According to the results of MD simulations, the stability of levothyroxine to AFP is quite remarkable. As a result of the interaction between tumor markers and drugs, molecular changes may complicate the detection of these molecules. The molecular changes in the structure of AFP in the AFP/levothyroxine complex quite possibly decrease the detection of serum AFP levels. Levothyroxine's interaction with CEA, CA 15-3, and especially with AFP molecules at low concentrations suggests that it may produce erroneous results in cancer patients undergoing diagnosis and treatment. The limitations of the study is that we only performed *in silico* analysis to show the binding of levothyroxine to the studied tumor markers. Experimental studies are necessary to validate the findings of the study, particularly those examining the effect of levothyroxine on the serum concentrations of CEA, CA 15-3, and AFP. Moreover, although this research hypothesizes a potential reduction in serum AFP levels due to

levothyroxine, this conclusion is exclusively derived from computational analyses. Therefore, experimental corroboration, including techniques like ELISA and immunological assays, is essential to ascertain its clinical relevance. As a consequence of this study, the amount of AFP that is present in the serum could appear to be quite low, which might lead to inaccurate findings. The misleading results of serum AFP levels in patients under diagnosis and cancer follow-up treatment could result in devastating outcomes.

Conflicts of interest

There are no conflicts of interest in this work.

Acknowledgements

Computing resources for Molecular Docking studies calculations reported in this paper were fully performed at Harran University High Performance Computing Center (Harran HPC resources). Computing resources used in this work for MD simulations were totally provided by the National Center for High Performance Computing of Turkey (UHeM) under grant number 1013972022.

References

[1] Taylor P.N., Global epidemiology of hyperthyroidism and hypothyroidism, *Nat. Rev. Endocrinol.,* 14(5) (2018) 301-316.
[2] Chiovato L., Magri F., Carlé A., Hypothyroidism in Context: Where We've Been and Where We're Going, *Advances in Therapy,* 36(S2) (2019) 47-58.
[3] Hughes K., Eastman C., Thyroid disease: Long-term management of hyperthyroidism and hypothyroidism, *Aust. J. Gen. Pract.*, 50(1-2) (2021) 36-42.
[4] Guerri G., *Hypothyroidism and hyperthyroidism*, Acta Biomed., 90(10-S) (2019) 83-86.
[5] Kravets I., Hyperthyroidism: Diagnosis and Treatment, *Am. Fam. Physician.*, 93(5) (2016) 363-70.
[6] Silsirivanit A., Glycosylation Markers in Cancer, *Adv. Clin. Chem.*, 89(2019) 189-213.
[7] Lee T., Teng T.Z.J., Shelat V.G., Carbohydrate antigen 19-9 - tumor marker: Past, present, and future, *World J. Gastrointest Surg.*, 12(12) (2020) 468-490.
[8] Seale K.N., Tkaczuk K.H.R., Circulating Biomarkers in Breast Cancer, *Clin Breast Cancer,* 22(3) (2022) e319-e331.
[9] Zhang M., Roles of CA125 in diagnosis, prediction, and oncogenesis of ovarian cancer, *Biochim. Biophys. Acta. Rev. Cancer,* 1875(2) (2021) 188503.
[10] Zheng Y., Zhu M., Li M., Effects of alpha-fetoprotein on the occurrence and progression of hepatocellular carcinoma, *J. Cancer Res. Clin. Oncol.,* 146(10) (2020) 2439-2446.
[11] Carlsson S.V., Vickers A.J., Screening for Prostate Cancer, *Med. Clin. North Am.,* 104(6) (2020) 1051-1062.
[12] Torres P.H.M., Key Topics in Molecular Docking for Drug Design, *Int. J. Mol. Sci.,* 20(18) (2019).
[13] Pinzi L., Rastelli G., Molecular Docking: Shifting Paradigms in Drug Discovery, *Int. J. Mol. Sci.,* 20(18) (2019).
[14] Akbaba E., Improvement of memory deficits via acetylcholinesterase inhibitory activity of Nepeta nuda ssp. nuda essential oil in rats, *Kuwait Journal of Science,* 48(3) (2021).
[15] Fu H., Accurate determination of protein:ligand standard binding free energies from molecular dynamics simulations, *Nat Protoc.*, 17(4) (2022) 1114-1141.
[16] Li J., Fu A., Zhang L., An Overview of Scoring Functions Used for Protein-Ligand Interactions in Molecular Docking, *Interdiscip Sci.,* 11(2) (2019) 320-328.
[17] Hollingsworth S.A., Dror R.O., Molecular Dynamics Simulation for All, *Neuron,* 99(6) (2018) 1129-1143.
[18] Suryandari D.A., Molecular Insights into Propylthiouracil as a Thyroid Peroxidase Inhibitor: A Computational Study Approach, *Indonesian Journal of Medical Chemistry and Bioinformatics*. 3(1) (2024).
[19] Li H., Integrated computational analysis of molecular mechanisms underlying perfluorooctane sulfonic acid induced thyroid toxicity, *Sci Rep.*, 15(1) (2025) 7920.
[20] Lu Y., Molecular Dynamic Simulation To Reveal the Mechanism Underlying MGL-3196 Resistance to Thyroxine Receptor Beta, *ACS Omega,* 9(19) (2024) 20957-20965.
[21] Pradhan S., Comparative Study on the Binding Affinity of Methimazole and Propylthiouracil to Thyroid Peroxidase as an Anti-Thyroid Drug: An Insilico Approach, *Journal of Molecular Imaging & Dynamics,* 07(01) (2017).
[22] Sandu N., Evaluation of the interaction of levothyroxine with bovine serum albumin using spectroscopic and molecular docking studies, *J. Biomol. Struct. Dyn.,* 40(3) (2022) 1139-1151.
[23] Xiong D., Comprehensive Analysis Reveals That ISCA1 Is Correlated with Ferroptosis-Related Genes Across Cancers and Is a Biomarker in Thyroid Carcinoma, *Genes (Basel),* 15(12) (2024).
[24] Gulfidan G., Systems biomarkers for papillary thyroid cancer prognosis and treatment through multi-omics networks, *Arch Biochem Biophys,* 715(2022) 109085.
[25] Mahmud S., Gene-expression profile analysis to disclose diagnostics and therapeutics biomarkers for thyroid carcinoma, *Comput Biol Chem.*, 113(2024) 108245.
[26] He Q., Combining Network Pharmacology with Molecular Docking for Mechanistic Research on Thyroid Dysfunction Caused by Polybrominated Diphenyl Ethers and Their Metabolites, *Biomed. Res. Int.,* 2021(2021) 2961747.
[27] Shih M.L., Large-scale transcriptomic analysis of coding and non-coding pathological biomarkers, associated with the tumor immune microenvironment of thyroid cancer and potential target therapy exploration, *Front Cell Dev. Biol.*, 10(2022) 923503.
[28] Morris G.M., AutoDock4 and AutoDockTools4: Automated docking with selective receptor flexibility, *J. Comput. Chem.*, 30(16) (2009) 2785-91.
[29] O'Boyle, Open Babel: An open chemical toolbox, *J. Cheminform,* 3(2011) 33.
[30] Akbaba E., Karatas D., Phytochemicals of Hibiscus sabdariffa with Therapeutic Potential against SARS-CoV-2: A Molecular Docking Study, *J. Inst. Sci. Technol.*, 13(2) (2023).
[31] Tang S., Sun L., Wang F., Identification of highly active natural thyroid hormone receptor agonists by pharmacophore-based virtual screening, *J. Biomol. Struct. Dyn.,* 39(3) (2021) 901-910.
[32] Bagci E., Evaluation of antiamnesic activity of Salvia multicaulis essential oil on scopolamine-induced amnesia in rats: in vivo and in silico approaches, *Heliyon,* 5(8) (2019) e02223.
[33] Dedon J., Thyroid Disease in Aging, Mo. Med., 119(4) (2022) 351-353.

[34] Hirasawa M., Interaction of Nevirapine with the Peptide Binding Groove of HLA-DRB1*01:01 and Its Effect on the Conformation of HLA-Peptide Complex, *Int. J. Mol. Sci.* 19(6) (2018).

[35] Behera S.K., In Silico Analysis Determining the Binding Interactions of NAD(P)H: Quinone Oxidoreductase 1 and Resveratrol via Docking and Molecular Dynamic Simulations, *Eur. J. Biol.,* 82(2) (2023) 280-288.

[36] Huang Y.H., CEACAM1 regulates TIM-3-mediated tolerance and exhaustion, *Nature,* 517(7534) (2015) 386-U566.

[37] Huang H.J., Lee C.C., Chen C.Y., Lead discovery for Alzheimer's disease related target protein RbAp48 from traditional Chinese medicine, *Biomed. Res. Int.,* 2014(2014) 764946.

[38] Rampogu S., Molecular Docking and Molecular Dynamics Simulations Discover Curcumin Analogue as a Plausible Dual Inhibitor for SARS-CoV-2, *International Journal of Molecular Sciences,* 23(3) (2022).

[39] Shoaib T.H., Exploring the potential of approved drugs for triple-negative breast cancer treatment by targeting casein kinase 2: Insights from computational studies, *Plos One*. 18(8) (2023).

[40] Zhang D., Lazim R., Application of conventional molecular dynamics simulation in evaluating the stability of apomyoglobin in urea solution, *Sci Rep.*, 7(2017) 44651.

[41] Johnson K.J., Cygan R.T., Fein J.B., Molecular simulations of metal adsorption to bacterial surfaces, *Geochimica Et Cosmochimica Acta.,* 70(20) (2006) 5075-5088.